Evaluation of the Radiosensitizing Capabilities of Target-Specific Gold Nanoparticles in the Radiotherapy of Prostate Cancer

Ana Marques

Instituto Superior Técnico, Lisboa, Portugal

December 2020

Abstract

The damages caused by radiation in healthy tissues in radiotherapy can be reduced by using radiosensitizers, such as gold nanoparticles, that increase the energy deposited in the cancer tissues while keeping the energy in the rest of the cells constant. This thesis studied this effect through computational and experimental work for both X-rays and Co-60 gamma rays. The Monte Carlo software PENELOPE was used to understand better the parameters influencing this effect, like the nanoparticle size, the type of radiation, and the beam width. In vitro procedures were performed in prostate cancer cells to quantify this effect and verify its evolution with time, such as micronuclei, MTT, and clonogenic assays after irradiation with 100 kVp X-rays and Co-60 gamma rays at two different dose rates. A different coating in the nanoparticle was also studied, specifically a bombesin coating that preferentially binds to the receptors existing in the prostate cancer cells used, allowing for a higher cellular uptake of the nanoparticles. The experimental results showed that high dose rates and the use of bombesin-coated nanoparticles increase the radiosensitization effect. A dose enhancement factor of 4.6 ± 1.8 was calculated from the simulations for the X-rays irradiation and 1.2 ± 0.4 for the Co-60 gamma rays irradiation.

Keywords: Gold nanoparticle, radiosensitization, radiotherapy, Monte Carlo

1. Introduction

Cancer is the second leading cause of death in the world and it was responsible for an estimated 9.6 million deaths in 2018 [1]. In Portugal, about 24.6% of all deaths in 2018 was due to cancer [2]. Specifically, prostate cancer is the second most commonly occurring cancer in men worldwide and the fourth most commonly occurring cancer overall [3].

Cancer is a large group of diseases involving modifications in the genome affected by interactions between the host and the environment. Typical characteristics of cancer are uncontrolled replication and the capacity to penetrate in other tissues, known as metastasis. Currently, the most widely used treatment modalities are surgery, chemotherapy, immunotherapy and radiotherapy. The selection of treatment depends on the type of cancer, its locality and stage of progression.

Radiotherapy consists on the deposition of energy in the cancer cells by irradiation (gamma rays, X-rays, electrons, protons or ions). The irradiation causes damages to the cancer cells themselves or their vasculature and thus cause cell death or nutrient starvation [4]. However, it is not possible to irradiate only the tumour cells, surrounding healthy tissue will also receive a considerable dose, because the mass energy absorption properties of cancer and healthy tissues are very similar [5]. It is therefore necessary to reduce the radiation dose delivered to the healthy tissues of the patient, while maximizing the dose delivered to the tumour. One way to do this is the use of radiosensitizers, which are defined as materials able to make tumour cells more sensitive to radiation. Metal-based nanoparticles represent an attractive option, as they absorb more energy per unit mass than soft tissue, increasing the local dose deposited in the tumour [5]. Specifically, gold nanoparticles (AuNPs) have several advantages, such as low cytotoxicity and effectiveness in dose enhancement [4].

The aim of this work is then to determine the potential benefit of combining radiation treatment with AuNPs, by studying the effects induced by radiation: gamma- and X-rays in prostate cell lines loaded with AuNPs. The cancer cell line that will be used is PC3 (prostate tumour). For this, both experimental and computational work has been developed. First, the cells were irradiated with Co-60 gamma rays for several dose points to obtain a survival curve. Afterwards, a specific dose was chosen for the cells to be irradiated with Co-60 and X-rays in the presence of AuNPs, and the in-

duced damages were studied, through clonogenic, micronucleus and MTT assays. Finally, a comparison between the effects induced by the AuNPs for two different dose rates is presented for Co-60 irradiation. For the simulation work, the Monte Carlo code used was PENELOPE (PENetration and Energy Loss of Positrons and Electrons) [6]. This software allowed for the estimation of the dose enhancement, a better understanding of this effect, and a confirmation of the experimental results.

2. Background

2.1. Biological Effects of Radiation

DNA is the main target for radiation-induced biological effects. Radiation can induce many lesions in the DNA molecules, however most are repaired by the cell. The typical damages are strand breaks (single and double). When the damages occur in one single strand of the DNA or both strands, but with breaks well separated, the cell can repair these lesions by taking the opposite strand as a template. However, when these damages occur in both strands and the distance between them is small (double-strand break or DSB), it can cleavage the chromatin into two separate pieces [7]. Clustered DNA damages and DSBs induced by radiation can then cooperatively contribute to cell death.

Most of the incident energy on the AuNP is actually transferred to the water surrounding it, leading to the production of radicals and other reactive species. Reactive Oxygen Species (ROS) have a short diffusion length, contributing to an increase in the local dose. The highest concentration of ROS will be therefore close to the surface of the AuNPs [8]. This oxidative stress is currently considered the primary cause of a radiosensitization effect in the MeV range, where the photoelectric absorption has a very small cross section [5].

2.2. Interaction of Radiation with Matter

Several physical processes are possible when ionizing radiation interacts with matter, different for uncharged and charged particles.

The most important interactions of photons with matter for radiotherapy purposes are the photoelectric effect, Compton scattering and pair production. The photoelectric effect consists of the absorption of the incident photon, followed by the emission of an electron from the target atom. The probability of this process is strongly dependent on the atomic number Z and the energy E of the photons. It is higher for high-Z materials and low-energy photons, varying as Z^4/E^3. The Compton effect refers to the scattering of the incident photon and the emission of an electron, and finally, pair production occurs when the incoming photon is converted into an electron-positron pair. Pair production becomes more probable with increasing photon energy, and it depends on the atomic number approximately as Z^2 [9]. For each material, the photoelectric effect is predominant for lower energies, the Compton scattering for intermediate energies and, finally, pair production for the highest energies.

After the atoms of the material are excited or ionized, they can de-excite through the emission of fluorescent photons or Auger electrons. For high-Z materials such as gold, the emission of fluorescent photons is favoured over Auger electron emission [9]. Auger electrons can, however, deliver a relatively high local dose, while fluorescent photons can travel farther in the tissue, causing a delocalization of the dose (typical attenuation lengths are in the order of the cm) [10]. The Auger effect is then a physical phenomenon in which the filling of an atom's inner-shell vacancy is accompanied by the emission of an electron from the same atom. For high-density media, Auger electrons have a typical range lower than 10nm. This Auger electron will propagate through the system, causing several secondary ionizations [11].

While uncharged radiations may traverse a medium and not interact at all, a charged particle interacts with one or more electrons or with the nucleus of almost every atom it passes, due to its Coulomb electric force field [12]. Beta particles (electrons/positrons) can excite and ionize atoms, radiate photons by bremsstrahlung, Cherenkov radiation and transition radiation, or directly interact with the Coulomb field of the nucleus (multiple scattering) [13]. The energy spent in radiative events is transported from the charged particle track, while that spent in collisions produces ionizations and excitations, contributing to the dose near the track [12].

2.3. Gold nanoparticles

Gold nanoparticles have several advantages as radiosensitizers, such as low cytotoxicity, effectiveness in dose enhancement due to the high atomic number of gold, and straightforward synthesis in a wide range of sizes [4]. One of the reasons gold is chosen is because of its mass attenuation and mass-energy absorption coefficients compared with that of soft tissue (or water). As seen in figure 1, this difference can reach two orders of magnitude in the keV region. Therefore, more secondary electrons will be produced in the gold that will deposit their energy close to the NP.

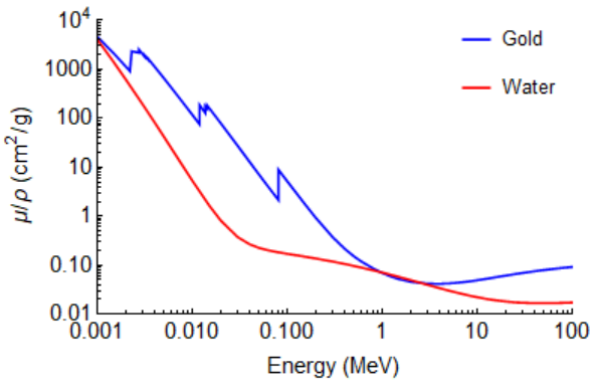

Figure 1: Plot of the mass attenuation coefficients for gold and water, with values taken from the NIST XCOM database.

One way AuNPs enter tumour tissues is by the Enhanced Permeability and Retention effect (EPR). The EPR effect describes the leaky tumour vasculature that originates from its rapid growth rate. Because of this, macromolecules such as NPs tend to accumulate within tumour tissue at higher concentrations than in healthy tissue.

The radiosensitization effect of NPs is quantified using the Dose Enhancement Factor (DEF), defined as the ratio between the dose absorbed by the tumour cells in the presence of the NPs and the dose absorbed in the absence of NPs [4].

$$DEF = \frac{D_{with\ gold}}{D_{without\ gold}} \quad (1)$$

The most important parameters to consider for the use of NPs in cancer therapy is their size and surface coating. These properties will determine their uptake inside the cells, their cytotoxicity, and their interaction with the incident radiation. The coating of NPs can be used to target the cancer cells. Specific membrane receptors, such as Gastrin Releasing Peptide receptors, are overexpressed in cancer cells and can be targeted with biomolecules with a high affinity towards them like bombesin (BBN) [14].

3. Experimental Methods

3.1. Cell culture

In this thesis, the cell line that will be studied is the PC3. This cell line was derived from bone metastases of grade IV prostate cancer, from a 62-year-old caucasian male [15]. Additionally, for one assay, the RWPE-1 cell line will be used. This was derived from a 54-year-old caucasian male.

The most important difference between these two cell lines, in the scope of this thesis, is that the tumorous cells have more GRP receptors in their membranes. This will cause the BBN-AuNPs to enter the tumour cells more easily and their concentration will be higher in these cells than in the healthy ones. Consequently, after irradiation, it is expected that there will be a higher radiosensitization effect in the tumour than in the healthy cells [16].

3.2. Gold nanoparticles

The AuNPs used in this thesis were coated with two different organic molecules, TDOTA and TA-BBN resulting in AuNP-TDOTA and BBN-AuNP-TDOTA respectively. BBN is a peptide that will help the AuNP to more easily enter the cells, thereby increasing its intracellular concentration. The AuNP-TDOTA had an estimated core size of (4.29 ± 1.60) nm and the BBN-AuNP-TDOTA of (4.79 ± 1.50) nm.

For the irradiation studies a preliminary evaluation of the cytotoxic effect of both AuNP-TDOTA and BBN-AuNP-TDOTA was done. Several AuNPs concentrations (gold content) were used and there was no cytotoxic effect in the range 2-75 μg Au/mL. The concentration 36 μg Au/mL was selected as a compromise to obtain a higher radiosensitizing effect with a negligible cytotoxic effect [17].

3.3. Irradiations

Some of the irradiations with Co-60 were performed in the Precisa-22 experimental irradiator (Graviner Manufacturing Company, Ltd) at CTN. The dose rate was chosen as 1 Gy/min and the uniformity of this value across the culture plates was verified. For the experiments with gold nanoparticles, the total dose in the cells was 2 Gy.

Another Co-60 irradiator was used (Eldorado 6, by AECL Medical Products) in the Metrology Laboratory of Ionising Radiation at CTN. At a distance of 1 m, with this irradiator, the dose rate was 25.7 mGy/min. In order to achieve the 2 Gy, the cells were irradiated for 78 mins. The uniformity of the dose rate was again guaranteed for the entire cell plate.

The irradiation with X-rays also took place in the Metrology Laboratory of Ionising Radiation at CTN. The system contained a Philips MCN 165 X-ray tube and a YXLON 9421 high-voltage generator. The ISO beam quality N100 was used, with a peak voltage of 100 kV and mean energy of approximately 84 keV, filtered with 4 mm Al and 5 mm Cu. The tube current was 20 mA and the distance from the cell plate to the source was 80 cm. With this irradiator, the cells received a total dose of 74 mGy at a dose rate of 1.23 mGy/min.

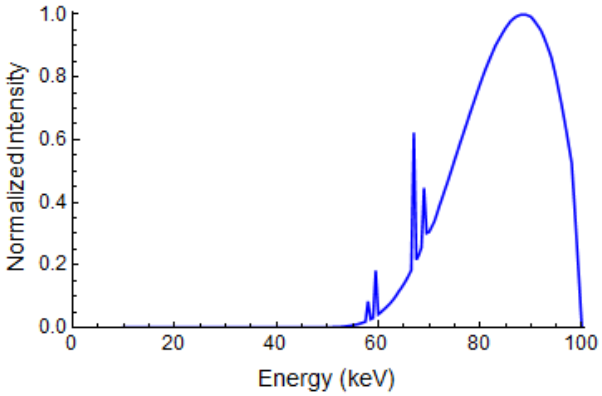

Figure 2: X-rays spectrum used for the experiments.

3.4. Assays

In a clonogenic assay, the reproductive ability of cells after irradiation is tested. The cells were incubated with the NPs approximately 3 hours before the irradiation. The cells were irradiated in 24-well plates, where each well contained a known number of cells. Immediately after irradiation, they were transferred to 6-well plates, to make it easier to discriminate the colonies after they are formed. They were then left to grow for 13 days in the incubator and afterwards the colonies were stained with a crystal violet solution and counted.

In the CBMN assay, following the irradiation, the cells were placed in the incubator for 22 hours. Then cytochalasin-B was added to each well at a concentration of 2 μg/mL to inhibit cytokinesis, the final stage of cell division, and they were returned to the incubator. After a total of 46h of incubation, the content of the wells for each dose was transferred to a 12 mL tube, carefully labelled. The tubes were then centrifuged, the supernatant was removed and the cells were washed with RPMI 1640 supplemented with FBS. The tubes were centrifuged again and the same procedure was repeated. Afterwards, the cells were subject to a mild hypotonic treatment, consisting of a mixture of RPMI 1640 and deionised water (1:4), supplemented with 2% FBS. The tubes were centrifuged one last time and the supernatant was removed. Small drops of the remaining cell pellet were placed in clean, dry slides, three for each dose, and the slides were left to air-dry overnight. The slides were then fixed with ice-cold methanol/acetic acid (3:1) for 20 minutes and stained with a crystal violet solution for 7 minutes. They were rinsed with tap water, dried and closed with Entellan.

In the MTT assay, the PC3 cells were seeded and allowed to adhere for 24 h. Then, a suspension of AuNPs with a concentration of 37 μg Au/mL was added to the cells and incubated for 2 h at 37ºC. After irradiation, the medium was discarded and the cells were maintained with fresh medium for 72 h. Afterwards the medium was removed and 200 μL of a MTT solution in PBS (0.5 mg/mL) was added to the cells and incubated for 3 h. The formazan crystals formed by the reduction of MTT were dissolved in DMSO. The absorbance was measured at 570 nm with a Elisa reader.

For all irradiations, clonogenic, micronucleus and MTT assays were performed. Additionally, a MTT assay was performed for the RWPE-1 cell line at Precisa-22, with the same dose and dose rate as for the PC3 cells, i.e. 2 Gy and 1 Gy/min.

4. Monte Carlo simulations

4.1. PENELOPE

PENELOPE is a Monte Carlo simulation code that describes the transport of photons, electrons and positrons in complex geometries, allowing the use of materials with arbitrary compositions. Its source code is written in Fortran-90 and it is continuously updated in the OECD Nuclear Energy Agency webpage. The version used for this thesis was PENELOPE2018. In the nanometric simulations performed, interaction forcing was used as a variance-reduction technique. It artificially increases the probability of an interaction to take place, in order to reduce the uncertainties of the simulation.

4.2. Simulations performed

In the first simulations, several parameters were varied and the results were analyzed. These parameters were the distance between the source and the NP, the beam width and the NP size.

For the tests varying the distance between the source and the NP, the DEF was calculated for 4 distances: 10^{-4} cm, 10^{-2} cm, 10^{-1} cm and 1 cm, in a sphere of radius 1 μm. There was a single NP with a diameter of 100 nm at the center of the tracking volume. The source was defined as a plane with a length of 110 nm, emitting a parallel beam. The cut-off energy for all particles was set at 50 eV. For Co-60, the spectrum consisted on the emission of gamma rays at 1.17 and 1.33 MeV. For the calculation of the X-ray spectrum, the program SpekCalc [18] was used to obtain a spectrum of 50 kVp X-rays, visible in figure 3. This spectrum was chosen for the first simulations to compare the results with other articles, such as [19].

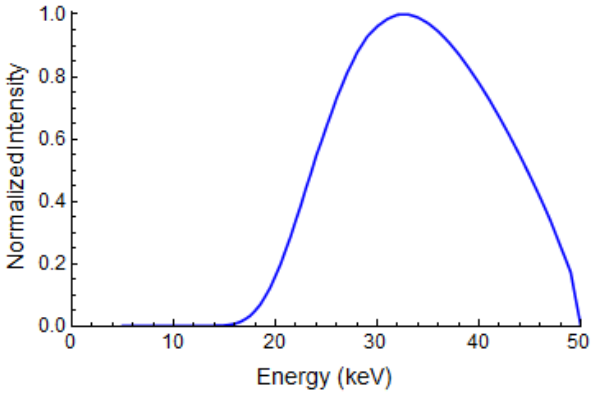

Figure 3: X-ray spectrum

The other parameters that were varied were the NP size as well as the beam width. Three different beam widths were chosen, 554, 654 and 800 nm. In this simulation, instead of the 1 μm shell, a simple cell model was used containing two concentric spheres to simulate the nucleus and the cytoplasm. Their dimensions were chosen to match an average PC3 cell, with the nucleus having a radius of 7.8 μm and the cytoplasm an outer radius of 11.3 μm. [20] In all of these simulations, the distance between the source and the NP was 50 μm.

Afterwards, some simulations were performed with several NPs in order to verify if using one bigger NP or a lot of smaller NPs will give the same DEF if the concentration of gold is the same. For this, simulations were made with a NP with a radius of 10 nm and 125 NPs with a radius of 2 nm each, corresponding to the same gold volume. The DEF was calculated in a water sphere with a radius of 100 nm. For the simulation with several NPs, they were randomly distributed in this 100 nm sphere, and for the simulations with one NP, it was placed in the centre of the sphere. The beam width was set to 200 nm and the distance from the source to the centre of the NP was 1 μm. This was performed only for X-rays because it requires less computational time to achieve reasonable uncertainties. The spectrum was approximately the one in figure 2.

The last simulations were the ones computed with the same parameters of irradiation as the experimental procedures. For this, a NP with a radius of 84.1 nm was computed to simulate the concentration of gold used in the experiments. Because this is a very localized effect, due to the very low range of the Auger electrons, instead of calculating the DEF in the whole cell, it was divided into shells. The shells had a thickness of 100 nm. For the Co-60 simulations, the distance between the source and the NP was estimated from the Precisa-22 irradiator and chosen as 21.91 cm. To reduce the computational time, a planar source was simulated instead of an isotropic one and the beam width was reduced to 1 and 5 μm. The spectrum used for the X-rays simulation was the one in figure 2. This spectrum was obtained assuming a thickness of air of 80 cm after the source and therefore, this distance was not added to PENELOPE. The distance between the source and the cell was then only 12 μm. The beam width was 50 μm for the NP with a radius of 84.1 μm and the cell with the radius of 11.6 μm. The world was again cubic with an edge of 25 cm.

5. Results

Based on the results of the experiments without gold nanoparticles, the total dose of 2 Gy was chosen for the studies with NPs, because this was a dose point with an intermediate value of cell death and a common dose in radiotherapy treatments with dose fractionation.

The results of the experimental part are presented in chronological order. The CBMN assay gives results of the damages in the DNA of the cells after one cell division. The MTT assay allows for the estimation of the cellular viability after 3 days (roughly 3 cellular divisions), while the clonogenic assay evaluates the survival of the cells after 13 days.

5.1. CBMN assay results

The results of the CBMN assay are in figure 4 for the three radiation sources. The results are calculated as the number of micronuclei divided by the number of scored binucleated cells (this ratio is called the micronuclei yield). These values are then normalized to each control.

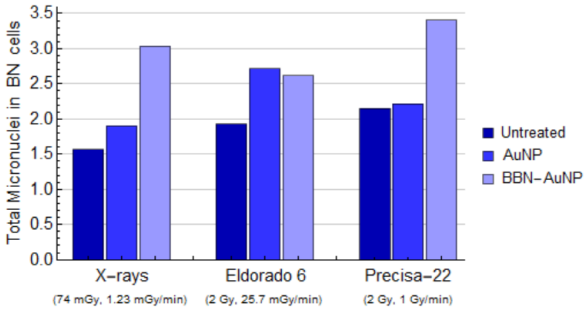

Figure 4: CBMN assay results for PC3 cells with varying doses.

The X-rays caused less damage because the total incident dose on the cells was lower. Regarding the effect of the NPs, there is a clear difference between the irradiated cells with and without AuNPs for X-rays and Co-60 gamma rays in the Eldorado 6 irradiator, but this difference is not significant in the Precisa-22 irradiator. However, when comparing the cells incubated with AuNPs and BBN-AuNPs, for X-rays and in Precisa-22, there is a clear

increase in the DNA damages for the PC3 cells with BBN-AuNPs. The radiosensitization effect of the NPs is proved in this assay. The samples incubated with BBN-AuNP with all three sources show more micronuclei than the irradiated cells without any NP. Compared to the irradiated PC3 cells, with the Eldorado 6 irradiator, there is an increase of 40% of the micronuclei yield; with Precisa-22, the increase is of the order of 60% and with X-rays, there is a 93% increase. It is possible to conclude that, even though the total dose in the cells with the X-ray irradiation is lower, the effect of the addition of BBN-AuNPs is higher for this radiation, as expected from the differences in the mass attenuation coefficient of gold and water (figure 1). Despite the fact that X-rays cause a higher radiosensitization effect of the AuNPs, the damages caused by this radiation are more easily repaired by the cell. The Co-60 gamma rays from Precisa-22, with the highest dose rate, is the radiation that causes a higher number of damages inside the cells. For PC3 cells only, around 7.5% of the binucleated cells had more than 1 micronuclei and this number increased to 11.5% when the cells were incubated with BBN-AuNPs. For X-rays, this value was around 2% and remained constant for cells with NPs. There is a clear higher damage in the cells after the Precisa-22 irradiation, however the damages caused by the X-rays are similar to those caused by the Eldorado 6 irradiation even though the dose in the cells in the latter is much higher.

5.2. MTT assay results

The MTT assay results are in figure 5. They were calculated as the ratio between the cellular viability in the irradiated sample and the cellular viability in the respective control. It is possible to conclude that after three days, there are no differences when comparing the three radiation sources. The cellular viability of the irradiated cells is the same in the three cases, when taking into account the uncertainties of the values. There is also no significantly higher radiosensitization effect of the BBN-AuNPs when compared to the AuNPs.

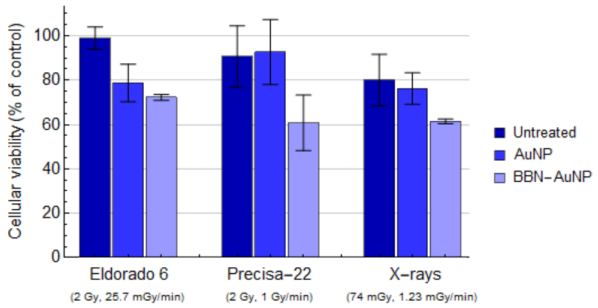

Figure 5: Cellular viability as a percentage of each control.

It can be seen however that there is a difference between the cells incubated with and without NPs. For X-rays and Co-60 gamma rays in the Eldorado 6 irradiator, there is a decrease of the cellular viability of around $(23 \pm 15)\%$ and $(27 \pm 5)\%$ respectively, when the irradiated cells were incubated with BBN-AuNPs. With the Precisa-22 irradiator, this decrease in the cellular viability was of the order of $(33 \pm 21)\%$.

Additionally, only for this assay, it was possible to perform the irradiation with RWPE-1 cells at Precisa-22. The cellular viability in this experiment was close to 100 % for the untreated cells and for the cells incubated with AuNPs and BBN-AuNPs. These results are as expected because tumourous cells have more receptors and the NPs will more easily enter the cells and cause more cell damage after irradiation.

5.3. Clonogenic assay results

The results are in figure 6. The effect of the irradiation remains as expected. For the X-ray irradiation, with the lowest dose in the cells, the survival of the PC3 cells is higher (approximately 70%). In the samples irradiated with Co-60 gamma rays, the total dose incident in the cells was higher and the survival fraction of the PC3 cells was around 50%.

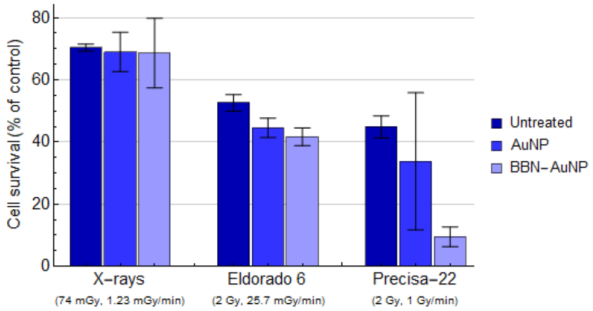

Figure 6: Cell survival as a percentage of each control.

It is possible to see that for the X-rays irradiation, the effect of the NPs has disappeared. The cell survival stayed constant independently of the initial incubation with AuNPs or BBN-AuNPs. For the irradiations with Co-60 gamma rays, although the variation between AuNPs and BBN-AuNPs is not significant, a difference can be seen between the cells without NPs and the samples with BBN-AuNPs. With Eldorado 6, there was a decrease of the survival fraction of $(21 \pm 7)\%$ in the cells with BBN-AuNPs. With Precisa-22, this decrease was of $(79 \pm 12)\%$.

5.4. Simulation results

The first simulation had the goal of studying the effect of the distance between the NP and the source

in the DEF, as well as seeing the difference between X-ray and Co-60 irradiations. The distances ranged from 1 μm to 1 cm. It was concluded that the DEF caused by X-rays is higher than the DEF caused by Co-60 gamma rays. The DEF ranged from 78 ± 3 to 64 ± 3 for X-rays and from 2.4 ± 0.5 to 1.5 ± 0.4 for Co-60. Additionally, for the distances considered, there is not a significant variation of the DEF with different distances.

For the next simulation, the AuNP diameter was changed for three different beam widths of 50 kVp X-rays. It can be seen from figure 7 that there is a linear relation between the DEF and the volume of the NP. The slope of this curve depends on the beam width, showing the importance of secondary particle equilibrium.

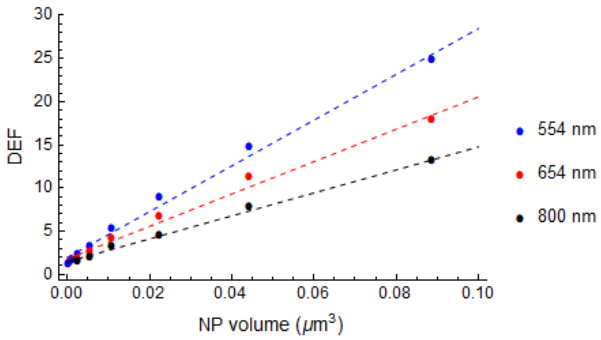

Figure 7: Effect of the variation of the NP size, for three different beam widths: 554, 654 and 800 nm.

This simulation had the cell divided into nucleus and cytoplasm in order to estimate the energy deposited in these bodies. In each one, the variation of the DEF followed the same tendency as the DEF in the overall cell but the DEF in the nucleus was bigger than the DEF in the cytoplasm. This happens because the NP is placed inside the nucleus and the low-energy secondary electrons, such as Auger electrons, that escape the NP will deposit their energy in the nucleus and only the particles with higher energy will leave the nucleus into the cytoplasm.

For the next simulations, the objective was to compare the DEF for 1 NP with a radius of 10 nm and for 125 NPs with a radius of 2 nm each. The results gave a DEF of 2.6 ± 0.4 for the 125 NPs and 2.1 ± 0.3 for the single NP. These values are in agreement with each other, because the uncertainty intervals overlap, and therefore it can be concluded that the DEF calculated for several smaller NPs can be approximated by the DEF for only one NP, if the bigger NP has the same volume as the summed volumes of the smaller NPs.

5.4.1 Simulations with the experimental conditions

The results are in figures 8 and 9 for X-rays and Co-60, respectively. In the shell immediately after the NP, as expected, is where the DEF is higher, quickly decreasing to 1 after only 500 nm. In the X-rays simulation, for a 1 μm beam, where secondary electron equilibrium does not exist, the DEF is 14 ± 2 and for a 50 μm beam, the DEF decreases to 4.6 ± 1.8. For Co-60, also for the 1 μm, the DEF is 1.8 ± 0.4, decreasing to 1.2 ± 0.4 for a 5 μm beam. It can be seen that, for the 5 μm beam of Co-60 gamma rays, there is no enhancement, not even in the first shell (considering however the very high uncertainties for the Co-60 simulations).

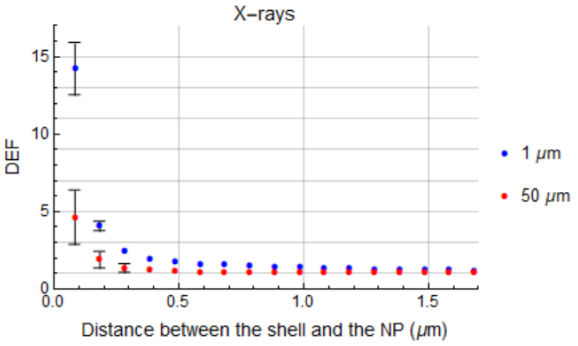

Figure 8: Variation of the DEF with the distance, for two different beam widths of 1 and 50 μm, with X-rays. Uncertainties below 5 and 20 % are not shown for the data points with the beam width of 1 and 50 μm respectively.

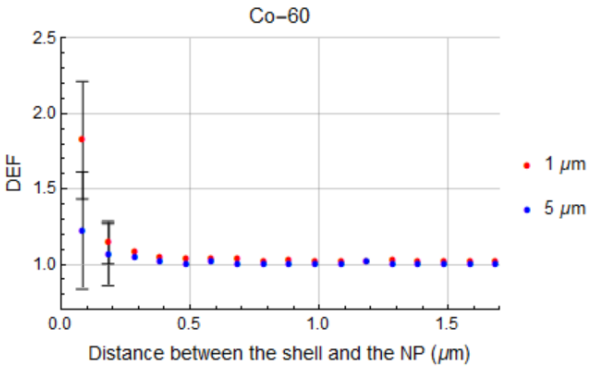

Figure 9: Variation of the DEF with the distance, for two different beam widths of 1 and 5 μm, with Co-60. Uncertainties below 10 and 15 % are not shown for the data points with the beam width of 1 and 50 μm respectively.

Additionally, the energy deposited on the first and second shells per particle type was recorded. For photons, this ratio is approximately 1 in both

simulations, but the ratio in the energies deposited by electrons is higher for X-rays, confirming that the dose enhancement is caused by the low-range Auger electrons. Furthermore, as expected, the DEF in the Co-60 simulations was very close to 1.

6. Discussion

In the following subsections, there are several comparisons that could be made from the experimental and computational results. It is important to mention that this work was affected by the pandemic. It was not possible to perform more assays, for example, to calculate or reduce uncertainties in the results.

6.1. Comparison between Co-60 and X-rays

From figure 4, the X-rays seem a better option for treatment with AuNPs because its effects are similar to those of gamma rays, but the total dose in the cells is much lower. However, the damages caused by gamma rays are harder to repair, i.e. the sum of all the micronuclei in the binucleated cells might be similar for X-rays and gamma rays, but for gamma rays, there are more clustered damages inside the cells. Therefore, with X-rays, the cancer cells might be able to repair themselves, and these damages might not necessarily lead to cell death, making the treatment ineffective. It can be seen in figure 5 that the cellular viability for the cells without NPs is similar in all three sources considering the uncertainty intervals. Regarding the effect of the NPs, it is very significant for the gamma rays in Eldorado 6, but for Precisa-22 the uncertainty intervals are too large for a conclusion to be made, as well as for the X-rays. Nonetheless, the decrease in cellular viability with the NPs is close for both X-rays and gamma rays, even though once again the dose in the cells irradiated with X-rays is much lower. Finally, the clonogenic assay allows for the estimation of cell survival after thirteen days. From figure 6, the cells under X-ray irradiation were the cells with the highest survival with values very close to those in the MTT assay. From this plot, the Co-60 gamma rays were the ones that caused more damages that, in the long term, caused cell death.

In conclusion, the effects caused by the NPs in the cells a few days after the irradiation are similar for X-rays and Co-60 gamma rays even if the total dose with X-rays was only 74 mGy and with gamma rays was 2 Gy. Therefore, in the short term, X-rays would be a better option for treatment. However, in the long term, the damages caused by the X-rays irradiation are more easily repaired by the cells. This suggests that using X-rays could not only be ineffective in killing the tumour cells, at least for the dose used here but also the effect of the addition of the NPs is not significant. Nonetheless, because there are effectively damages in the nucleus of the cells in the first days, a good option would be to increase the total dose in the cells or to perform a treatment with dose fractionation. This would give the healthy cells around the tumour a higher chance of repairing their damages and create more clustered damages in the cancer cells. In the long term, the Co-60 gamma rays prove to be a better treatment option, as they lead to smaller cell survival in figure 6, for the doses used. Even though, physically, the effect occurs only for X-rays irradiation, it can be seen in these results that there is an effect even with Co-60 irradiation that cannot be explained by the different mass-energy absorption coefficients for gold and water as for X-rays. The effect still occurs, most likely, due to ROS production.

6.2. Comparison between AuNPs and BBN-AuNPs

From the CBMN assay, in figure 4, it can be concluded that one day after the irradiation, there is an increased radiosensitization effect of the BBN-AuNPs compared to that of the AuNPs in the PC3 cells, for two of the three irradiation sources studied, as this difference does not occur in the Eldorado 6 irradiator. Two days later, in the MTT assay, there is indeed a higher dose enhancement effect with BBN-AuNPs in two of three radiation sources, even three days after the irradiation. The effect is still not visible for the Eldorado 6 irradiation. In the last assay, there is no significant difference in the cell survival between the cells incubated with AuNPs and BBN-AuNPs in all three sources, although the irradiated cells with AuNPs in Precisa-22 show a very high variation of the survival results, leading to a very high uncertainty in this value. Consequently, it can be concluded that thirteen days after the irradiation, the higher number of damages in the cells seen from the CBMN assay in the samples with BBN-AuNPs disappears, as the damages were repaired by the cells. In short, there is, in fact, a higher radiosensitization effect when BBN-AuNPs are used, because their uptake into the cells is higher. However, this effect increases the damages inside the cells only a few days after the irradiation. After a more extended period of time, there is no difference in the cell survival between the cells with AuNPs and the cells with BBN-AuNPs.

6.3. Comparison between dose rates

As mentioned in section 4, the Precisa-22 irradiations were performed at a dose rate of 1 Gy/min, while with the Eldorado 6 irradiator, a dose rate of 25.7 mGy/min was used. The cells received the same total dose. In the CBMN assay, the micronuclei yield in binucleated cells is higher in the cells incubated with BBN-AuNPs for the highest dose rate; however, it is lower for this dose rate when they are incubated with AuNPs. The damages are harder for the cell to repair when a high dose rate is

used. From the MTT assay, the results are very similar between the two dose rates. In the clonogenic assay, the effect of the BBN-AuNPs is very pronounced in the irradiation with Precisa-22, at the highest dose rate, however, there is still a decrease in the cell survival for the Eldorado 6 irradiations when the cells were incubated with BBN-AuNPs. To summarize, the radiosensitization effect of the BBN-AuNPs is increased when a high dose rate of Co-60 gamma rays was used. It is evident from these results that, when studying the dose enhancement caused by NPs, the dose rate is a parameter just as crucial as the total dose in the cells.

6.4. Comparison between experimental and computational work

The computational results will be compared to the results of the CBMN assay for the cells incubated with BBN-AuNPs. The spectra used in both situations, Co-60 and X-rays, was approximately the same between the simulations and experimental procedures. The concentration of NPs used in the simulations was 37.5 μg/mL while the experimental one was 36 μg/mL.

For X-rays the experiments showed that the irradiated cells with BBN-AuNPs had twice more damages than the irradiated cells without NPs. On the other hand, the simulated DEF was 4.6 ± 1.8 in the first shell after the NP for the largest beam. These results cannot be compared directly because a few approximations were used in the simulations that affect the results, the biggest being the NP itself. While it was proved that using several NPs or one bigger NP does not significantly alter the DEF, it cannot be concluded that, biologically, having one bigger NP or a lot of smaller ones causes the same damages. Additionally, the simulations assumed not only 100 % cellular uptake but also 100 % uptake into the nucleus, two reasons that can explain the higher value of the DEF in the simulations.

For Co-60, in the experimental part, the irradiated cells with BBN-AuNPs had 1.5 times more damages than the irradiated untreated PC3 cells. In the simulation, the DEF obtained with the largest beam was 1.2 ± 0.4 in the first shell around the NP, indicating no radiosensitization effect. Although these results are very different from each other, it is what was expected, because the effect caused by the NPs after Co-60 irradiation cannot be explained by the physical interaction of the photons with the cells, but instead, they are based on the chemical reactions happening after the initial ionizations, which the software used does not compute.

Overall these simulations give a general idea of how specific parameters influence the dose enhancement effect, such as the NP size and type of radiation, but cannot yet provide an estimation of the value of the DEF. For this, a better option would be, for example, to use Geant4-DNA, which also contains processes for the modelling of biological damage induced by ionizing radiation at the DNA scale.

7. Conclusions

This thesis had the objective of studying the radiosensitization effect of AuNPs in PC3 cells. According to the obtained simulation results, there is a radiosensitization effect caused by the difference in the mass-absorption coefficients of gold and water and therefore depending on the energy of the incident photons. This effect is higher for keV energies and lower for MeV energies, such as the energies of Co-60 gamma rays, as verified in the simulation results.

When performing simulations with approximate parameters as the experimental irradiations, the results gave a DEF of around 5 for X-rays and 1 for Co-60, in a 100 nm shell immediately after the NP, proving again the difference between the two types of radiations. However, these results are hard to compare to the experimental values obtained due to the several approximations/limitations in the simulations.

The experimental part concluded that BBN-AuNPs show a higher dose enhancement effect than simple AuNPs. Furthermore, a small dose of 74 mGy in the cells, from X-ray irradiation, led to a significant radiosensitization effect in the short term, however after thirteen days had passed, the effect was no longer visible. For Co-60 irradiation, it was concluded that a high dose rate improved the dose enhancement from the NPs. An MTT assay of RWPE-1 cells after irradiation with Precisa-22 proved the low radiosensitization effect in normal healthy cells due to the low number of receptors in these cells' membranes and consequently the low concentration of NPs inside them.

8. Future Work

Regarding the computational work, a few ideas for future improvement are: using different Monte Carlo codes to compare the results of the simulations, such as Geant4 or MCNP, specifically use a Monte Carlo software that also simulates the production of ROS, in order to have a more realistic value of the DEF; and including different distributions of the AuNPs in the cells instead of adding them only to the nucleus.

In the experimental field, to improve these results, these experiments should be performed for the same total dose in the cells for X-rays and Co-60 gamma rays, and it would be interesting to perform the same assays for healthy prostate cell lines, such as RWPE-1. Additionally, a few interesting ideas would be a study on the effect of dose fractiona-

tion in the radiosensitization of the NPs, evaluate the mitochondrial damages caused by NPs, as these can also lead to cell death and see this effect for different particle beams, such as electron or proton beams.

Acknowledgements
This work was developed in the framework of NANOGLIO (PTDC/MED-QUI/29649/2017), funded by Fundação para a Ciência e Tecnologia (FCT, Portugal), and the TOF-PET FOR PROTON THERAPY (TPPT) project, funded by FCT and ANI (045904).

References

[1] World Health Organization. Cancer. https://www.who.int/news-room/fact-sheets/detail/cancer, 2018. [Online; accessed 23-November-2019].

[2] Pordata. Óbitos por algumas causas de morte (%). https://www.pordata.pt/Portugal/, 2019. [Online; accessed 24-November-2019].

[3] World Cancer Research Fund. Prostate cancer statistics. https://www.wcrf.org/dietandcancer/cancer-trends/prostate-cancer-statistics. [Online; accessed 24-November-2019].

[4] K. Haume, S. Rosa, S. Grellet, M. Śmiałek, K. Butterworth, A Solov'yov, K. Prise, J. Golding, N. Mason. Gold nanoparticles for cancer radiotherapy: a review. *Cancer Nanotechnology*, 7:8, 11 2016.

[5] S. Rosa, C. Connolly, G. Schettino, K. Butterworth, K. Prise. Biological mechanisms of gold nanoparticle radiosensitization. *Cancer Nanotechnology*, 8, 12 2017.

[6] J. Sempau, A. Badal, L. Brualla. A PENELOPE-based system for the automated Monte Carlo simulation of clinacs and voxelized geometries—application to far-from-axis fields. *Med. Phys.*, 38:5887 – 5895, 2011.

[7] E. J. Hall, A. J. Giaccia. *Radiobiology for the Radiologist*. Wolters Kluwer Health, 2018.

[8] B. J. Choi, K. O. Jung, E. E. Graves, G. Pratx. A gold nanoparticle system for the enhancement of radiotherapy and simultaneous monitoring of reactive-oxygen-species formation. *Nanotechnology*, 29(50):504001, oct 2018.

[9] J. Turner. *Chemical and Biological Effects of Radiation*, chapter 13, pages 399–447. John Wiley & Sons, Ltd, 2007.

[10] H. Byrne, Y. Gholami, Z. Kuncic. Impact of fluorescence emission from gold atoms on surrounding biological tissue - implications for nanoparticle radio-enhancement. *Physics in medicine and biology*, 62, 02 2017.

[11] L. Cederbaum V. Stumpf, K. Gokhberg. The role of metal ions in x-ray induced photochemistry. *Nature Chemistry*, 8, 05 2015.

[12] F. H. Attix. *Gamma- and X-Ray Interactions in Matter*, chapter 7, pages 124–159. John Wiley & Sons, Ltd, 2007.

[13] A. De Angelis, M. Pimenta. *Introduction to Particle and Astroparticle Physics: Multimessenger Astronomy and its Particle Physics Foundations*. Undergraduate Lecture Notes in Physics. Springer International Publishing, 2018.

[14] A. Araneda. *Development of a Methodology for the Determination of a TXRF Spectrometer Sensitivity Curve*. PhD thesis, 04 2015.

[15] ATCC. Cells and microorganisms. https://www.lgcstandards-atcc.org/Products. [Online; accessed 20-August-2020].

[16] R. Markwalder, J. C. Reubi. Gastrin-releasing peptide receptors in the human prostate. *Cancer Research*, 59(5):1152–1159, 1999.

[17] F. Silva. *Gallium Compounds for the Design of (Nano)radiopharmaceuticals*. PhD thesis, Faculdade de Ciências da Universidade de Lisboa, 2014.

[18] G. Poludniowski, G. Landry, F. DeBlois, P. M. Evans, F. Verhaegen. SpekCalc: a program to calculate photon spectra from tungsten anode x-ray tubes. *Physics in Medicine and Biology*, 54(19):N433–N438, sep 2009.

[19] W. B. Li et al. Intercomparison of dose enhancement ratio and secondary electron spectra for gold nanoparticles irradiated by X-rays calculated using multiple Monte Carlo simulation codes . *Physica Medica: European Journal of Medical Physics*, 69:147 – 163, 2020.

[20] M. C. Kolios, G. J. Czarnota. High frequency ultrasound scattering from mixtures of two different cells lines: Tissue characterization insights. *Physics Publications and Research*, 11, 2008.